

S. Burgmann · C. Brücker · W. Schröder

Scanning PIV measurements of a laminar separation bubble

Received: 10 November 2005 / Revised: 11 April 2006 / Accepted: 11 April 2006 / Published online: 11 May 2006
© Springer-Verlag 2006

Abstract Scanning PIV is applied to a laminar separation bubble to investigate the spanwise structure and dynamics of the roll-up of vortices within the bubble. The laminar flow separation with turbulent reattachment is studied on the suction side of an airfoil SD7003 at Reynolds numbers of 20,000–60,000. The flow is recorded with a CMOS high-speed camera in successive light-sheet planes over a time span of 1–2 s to resolve the temporal evolution of the flow in the different planes. The results show the quasi-periodic development of large vortex-rolls at the downstream end of the separation bubble, which have a convex structure and an extension of 10–20% chord length in the spanwise direction. These vortices possess an irregular spanwise pattern. The evolution process of an exemplary vortex structure is shown in detail starting from small disturbances within the separation bubble transforming into a compact vortex at the downstream end of the separation bubble. As the vortex grows in size and strength it reaches a critical state that leads to an abrupt burst of the vortex with a large ejection of fluid into the mean flow.

deployed slat. Especially due to the growing research in the field of small unmanned air vehicles (UAV), which are typically cruising at relatively low Reynolds numbers, laminar airfoil flows become of more and more interest. Usually, the tendency for flow separation under such conditions is more critical than for large-scale airfoils, degrading massively the performance and stability of the UAV (McMichael and Francis 1997).

For airfoils at low Reynolds numbers a locally confined flow separation with a turbulent reattachment closing the separated region can be observed (O'Meara and Mueller 1987). The laminar boundary layer detaches due to an adverse pressure gradient. Kelvin–Helmholtz instabilities occur, leading to a roll-up of the separated shear layer such that vortex structures evolve in the vicinity of the reattachment region. Usually the flow of a separation bubble exhibits a complex temporal behavior and mutual interaction with the mean flow, as shown in numerical studies, e.g., by Pauley et al. (1990) and Maucher et al. (1994) as well as in experimental investigations, e.g., by Gaster (1966) or Watmuff (1999).

To control a laminar separation bubble a good physical understanding is essential, which requires a detailed knowledge of the time-dependent three-dimensional flow evolution within the separation bubble as well as in the upstream and downstream regions. Considering time-resolved and three-dimensional studies on a laminar separation on the suction side of an airfoil there are hardly any publications in the literature. Only recently, some thorough experimental investigations have been carried out using hot-wire probes (Watmuff 1999), laser-Doppler-anemometry and particle-image-velocimetry (Lang et al. 2004; Hain and Kähler 2005). Watmuff (1999) and Lang et al. (2004) investigated the separation bubble that emerges on a flat plate due to an adverse pressure gradient while Hain and Kähler (2005) analyzed the separation bubble that develops on the suction side of an SD7003 airfoil. Only the results given by Lang et al. and Hain and Kähler are able to give an impression of the three-dimensional flow structures in time and space by means of flow visualization and

1 Introduction

Low Reynolds number flows in the order of $O(10^4\text{--}10^5)$ are of major concern for some significant aerodynamic applications, e.g., turbomachine blades or flow around a

S. Burgmann (✉) · W. Schröder
Department of Fluid Mechanics, Institute of Aerodynamics,
RWTH Aachen University, Wüllnerstrasse zw. 5 u. 7,
52062 Aachen, Germany
Tel.: +49-241-8095569
Fax: +49-241-8092257
E-mail: s.burgmann@aia.rwth-aachen.de
URL: www.aia.rwth-aachen.de

C. Brücker
Institute of Mechanics and Fluid Dynamics, TU Freiberg,
Lampadiusstraße 4, 09596 Freiberg, Germany

phase-averaged PIV-measurements and conventional PIV-measurements, respectively. So the spatial structure of the separation bubble on an airfoil is not completely investigated and to fully understand the dynamic behavior of the laminar separation bubble on an airfoil time-resolved and three-dimensional measurements are a must. Therefore we use in this work time-resolved PIV and scanning PIV (SPIV) (Brücker 1997) to capture the spatial and temporal evolution of the vortex dynamics at the downstream end of the separation bubble. Regarding the application of PIV, this is a straightforward task due to the small aspect ratio and the high-velocity gradients within this region (Raffel et al. 1998). In this paper, we focus on the three-dimensional and temporal resolution of a laminar separation bubble, which is generated at the suction side of a laminar airfoil SD7003 at low Reynolds numbers and at moderate angles of attack between 4° and 8° . The paper is organized as follows. First, the experimental method is described. Subsequently, the flow field is analyzed based on PIV measurements in differently oriented cross-sections. In the final section, an overall discussion leading to a qualitative model of the separation structure is presented and a conclusion is given.

2 Experimental method

PIV measurements of the laminar separation on the suction side of the SD7003 airfoil were performed in a Göttingen type water tunnel with a cross-section of $300 \text{ mm} \times 250 \text{ mm}$ (Fig. 1) at Reynolds numbers based on the chord length ($c = 200 \text{ mm}$) of $Re_c = 20,000\text{--}60,000$ and angles of attack of $\alpha = 4\text{--}8^\circ$. This type of airfoil was chosen since a long-stretched laminar separation bubble occurs over a broad range of angles of attack at Reynolds numbers below 100,000 (Selig et al. 1995). The airfoil with a transparent segment in the spanwise center was mounted between the upper and lower wall of the tunnel to avoid disturbances of the wing tip vortices with the separation bubble (Bastedo and Mueller 1986). Due to the relatively small thickness

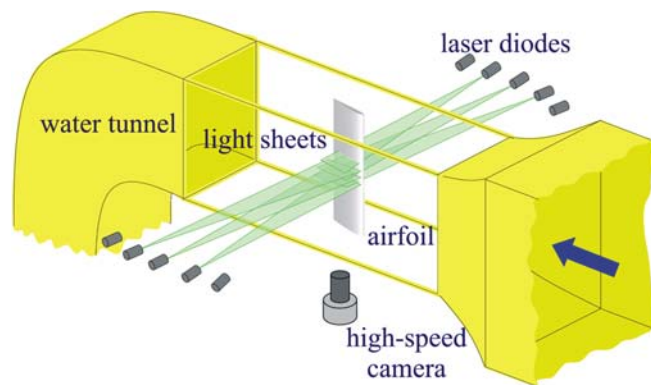


Fig. 1 Sketch of the water tunnel with the model and the laser sheet scanning system

of $0.0851c$ the blockage effect can be neglected. To characterize the spatial and temporal evolution in the separation region, the standard time-resolved PIV and the SPIV method were applied in selected regions of the separation bubble. For all measurements, images were recorded with a CMOS high-speed camera at frame rates between 308 and 922 Hz and a resolution of $1,024 \times 512$ pixels. The light-sheet illumination system consisted of ten adjustable laser diodes each of which had a power of 50 W in continuous mode at a wavelength of 805 nm (Fig. 2). All diodes could be adjusted and positioned independently. A special electronic control allowed to pulse the laser diodes in any desired sequence or simultaneously. The frame capture signal was synchronized with the pulse control such that each image in the sequence corresponded to a pulse of a certain laser diode.

First, time-resolved 2C-PIV measurements were taken in a single light sheet positioned in the flow direction and perpendicular to the airfoil surface to detect the local streamwise and spanwise expansion and the dynamic behavior of the separation bubble. For these measurements only one single laser diode in pulsed mode was used. The flow field around the airfoil was covered with three slightly overlapping measurement regions. To resolve the dynamic behavior an enlarged area of the reattachment region was investigated. Next, SPIV measurements were done using different orientations of the scanning light sheets. Firstly, the scanning planes were orientated parallel to the main flow and perpendicular to the airfoil surface and secondly, the light sheets were located parallel to the airfoil surface. In the first experiments, the flow was scanned in the spanwise direction starting from the midplane of the airfoil model in five parallel planes with a spacing of $\Delta z = 2.5 \text{ mm}$ yielding a total scanning width of $\Delta_{\text{scan}} = 10 \text{ mm}$. In the second measurements, three scanning planes were used with $\Delta z = 1.5 \text{ mm}$ and $\Delta_{\text{scan}} = 4.5 \text{ mm}$. The illuminated two-dimensional area is moving stepwise through the measurement volume,

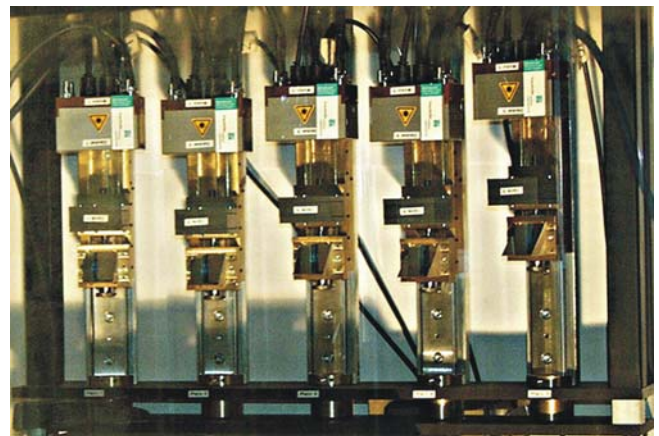


Fig. 2 Photograph of laser sheet scanning system; rack for five laser diodes

starting with the first plane after each scanning-cycle. The PIV post-processing was done with a cross-correlation of images of the same plane, i.e., one image is correlated with the subsequent fifth and third image, respectively. Since the scanning time is proportional to the number of desired planes, the maximum flow speed has to be adjusted such that the particles remain within the interrogation windows in the correlated images that are images of the same plane. In other words, this limits either the number of planes or the flow speed. In addition, the limited depth of focus of the recording lens, which restricts the total scanning width, has to be taken into account. In our case, we chose a long focal lens ($f = 105$ mm) and relatively large polystyrol tracer particles with a mean diameter of 20 μm .

In general, the PIV data were post-processed using an adaptive cross-correlation starting with 32×32 pixels interrogation windows with window shifting and window reduction, which leads to 16×16 pixel interrogation windows with 50% overlap, i.e., 128×64 vectors per image.

The following table shows in detail the features for each measurement (Table 1).

3 Results

In this section, we focus on the total flow around the airfoil such that the location of the separation bubble can be detected in the first part. Next, the two-dimensional time-resolved PIV results of the flow in the reattachment region within the separation bubble are shown. Finally, the results of the SPIV measurements in the reattachment region are presented using several planes in the spanwise and wall-normal direction.

In the following, exemplary results are shown for a freestream velocity of $u_\infty = 10$ cm/s and an angle of attack of $\alpha = 6^\circ$. Under such conditions the separation bubble is located between $x/c = 0.25$ and 0.55 , where the surface of the suction side of the airfoil is approximately planar. Although larger freestream velocities are possible the study focuses on the lower freestream velocity of $u_\infty = 10$ cm/s to enable a larger number of planes in the SPIV measurements. A global picture of the mean flow over the airfoil is given in Fig. 3, which is based on the average of 1,000 images in three slightly overlapping recording regions.

The boundary layer thickness near the separation is in the order of $\delta_0 = O(6$ mm), which is slightly larger

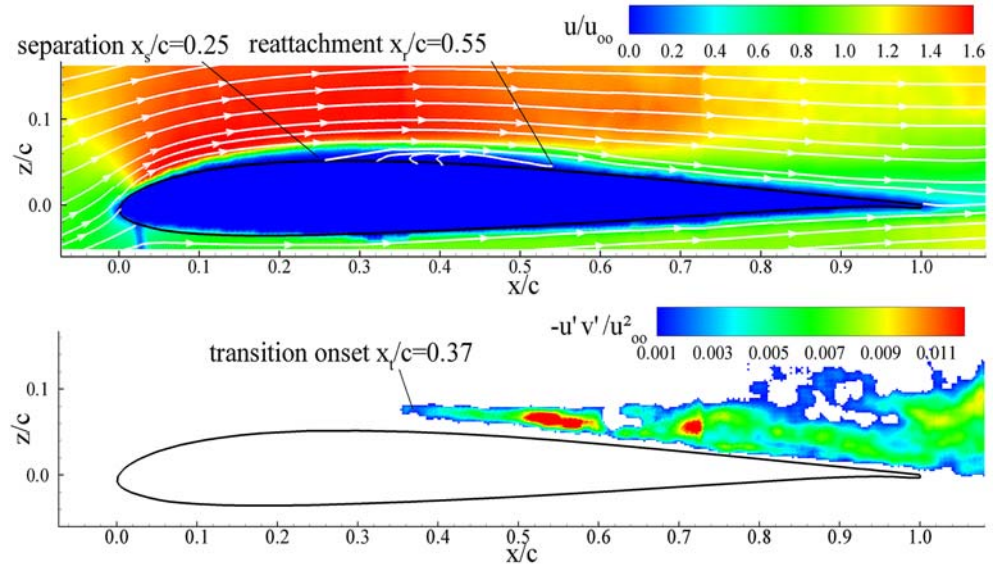
than the maximum bubble thickness $\delta_{\text{bub}} = O(4$ mm). Furthermore, the streamwise extent of the total separation region is in the order of $O(10\delta_0)$. The size of the separation bubble is evidenced by the mean velocity distribution and the calculated streamlines in the separation region (Fig. 3). The locations, where separation starts and reattachment occurs, are cross-checked by investigating the particle movements in the original particle images. The lower part of Fig. 3 displays the contours of the normalized Reynolds shear stresses above a critical value of 0.001. This value is chosen in the literature, e.g., by Ol et al. (2005), to locate the onset of transition in the separated shear layer. In our investigation the onset occurs approximately near $x/c = 0.37$.

Due to the shear layer roll-up in the outer region of the separation bubble, regions of concentrated vorticity are formed, which interact with the downstream part near the reattachment point. In addition, via the pressure distribution this process has a feedback on the separation bubble itself leading to a complex mutual interaction, i.e., a temporal change of the length and thickness of the separation bubble and an influence on the vortex size and strength. Figure 4 displays a series of vector fields over a time span of 2.2 s for $u_\infty = 10$ cm/s and $\alpha = 6^\circ$. The roll-up process starts with a small disturbance upstream in the separation bubble (Fig. 4 at t_0). At increasing time, the small disturbance grows and vorticity accumulates until a large vortex is formed, which is located approximately $O(4\delta_0)$ upstream of the reattachment line, e.g., vortices no. 2 and no. 3 in Fig. 4 at $t_0 + \Delta t$ and $t_0 + 2\Delta t$. This phenomenon of vortex formation and drift was also observed by Watmuff (1999) and calculated by Pauley et al. (1990) defined as ‘‘vortex shedding.’’ The vortex travels downstream at approximately 60% of the freestream velocity u_∞ , which is of the same size as the calculated drift speed of 65% given by Pauley et al. (1990). The vortex continues its drift until it reaches a critical condition, which forces the vortex to burst. This bursting process is seen as an abrupt strong vertical fluid ejection into the mean flow, see vortex no. 1 and no. 3 at $t_0 + \Delta t$ and $t_0 + 5\Delta t$. Occasionally, some vortices pair like vortex no. 3 with no. 4 ($t_0 + 5\Delta t$) and burst right after pairing. The bursting is a consequence of a sometimes only slight decrease of the downstream speed of the vortex, the simultaneous accumulation of vortex strength, and the growing size of the vortex until a critical condition is reached, which is assumed to be defined, among other

Table 1 Technical details of the PIV-measurements

Measurement case	In-plane resolution (mm/pixel)	Measurement volume (mm^3)	Vectors per plot	Particle-image diameter	Particle-image density per 32×32 pixels
Global view	0.075	–	$\approx 23,000$	2–3 pixels	≈ 11
Detail view	0.033	–	8,192	3–4 pixels	≈ 8
Spanwise scan	0.033	$33.8 \times 16.9 \times 10.0$	$5 \times 8,192$	3–4 pixels	≈ 8
Wall-normal scan	0.185	$189.4 \times 94.7 \times 4.5$	$3 \times 8,192$	1–3 pixels	≈ 20

Fig. 3 Contours of mean streamwise velocity with streamlines (top) and Reynolds shear stresses $-u'v'/u_\infty^2$ (bottom) for $u_\infty = 10$ cm/s and $\alpha = 6^\circ$; the separation and reattachment points are derived from the near-wall streamlines

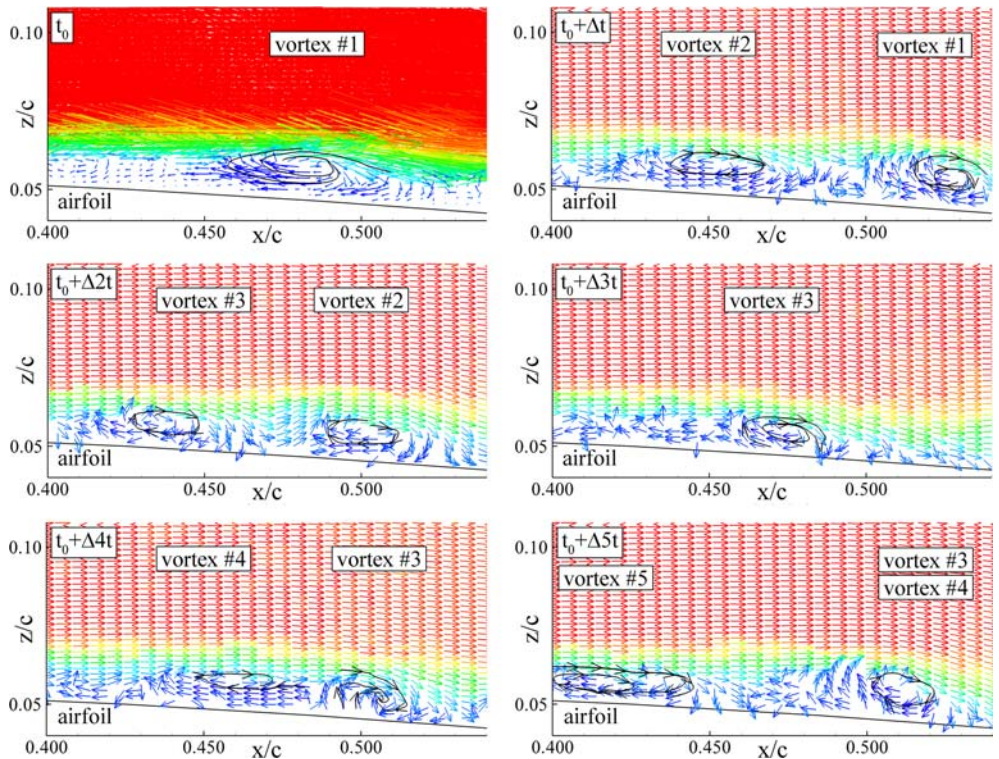


criteria, by the ratio of the tangential and normal momentum flux. The burst itself looks as if the vortex packet as a whole turns around the reattachment point in a tumble-like motion. A vortex loop with a detachment of the vortex from the airfoil surface as observed by Watmuff (1999) was not found.

A visualization of the dynamic behavior in this region is shown in Fig. 5 by means of strip charts, which display the spatio-temporal reconstruction of the magnitude of the vertical velocity component along a line normal to the surface at the streamwise locations

$x/c = 0.45, 0.47, 0.5$ and 0.52 . The data are taken from the time-resolved PIV results. The red color indicates a relatively large v -component away from the surface, that is an ejection and the blue color indicates motion towards the surface wall, called sweep. The structures in the strip charts correspond to the vertical fluid motion of the vortex passing the corresponding locations A–D. They are to a certain extent related to the vector plots in Fig. 4. It turned out that the velocity disturbances extend far into the outer flow region. The temporal reconstruction shows a number of four vortices starting

Fig. 4 Evolution process from t_0 to $t_0 + 5\Delta t$ of finally bursting large-scale vortices; time interval between pictures $\Delta t \approx 200$ ms. Vortices are indicated by streamlines. Vectors are drawn with uniform length except in (a) where proportional vector length is used



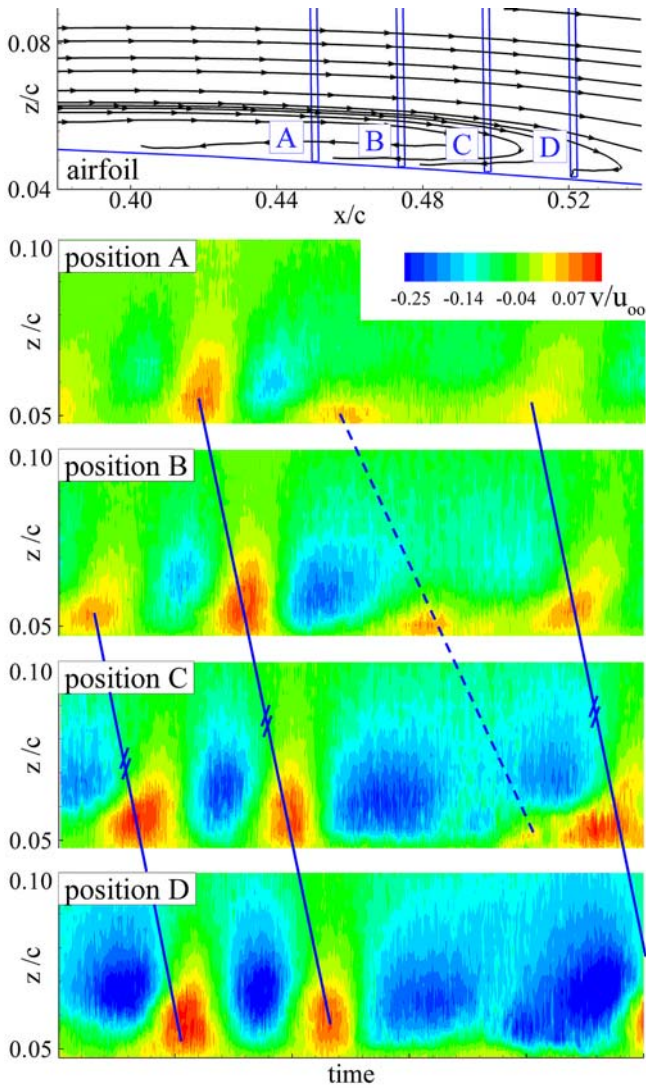


Fig. 5 Strip charts of the spatio-temporal reconstruction of the magnitude of the vertical velocity component

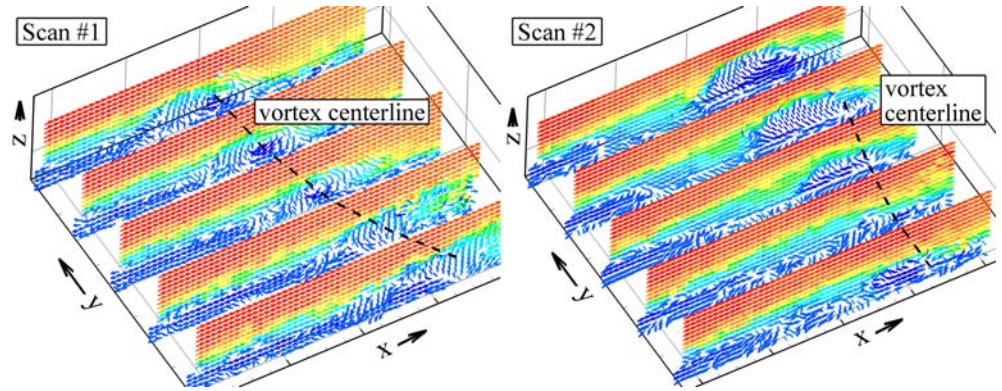
with an almost regular pattern over the whole recording period of 2.2 s (Fig. 5, position A). From the number of images from vortex no. 1 through vortex no. 4 and the recording frequency of 461 Hz the vortex roll-up frequency can be obtained, which is approximately 2.6 Hz for $u_\infty = 10$ cm/s and $\alpha = 6^\circ$. The vortex roll-up frequency denotes the temporal formation of vortices at the end of the separation bubble. The vortices possess a downstream velocity which is equal to roughly 60% of the freestream velocity. When they propagate from the upstream location of the separation bubble the intensity of vertical motion increases as evidenced in Fig. 5 by the change of the color from bright to deep red and bright to deep blue, respectively. Most of the vortices keep their downstream speed (no. 2 and no. 4), whereas some vortices decelerate, leading to vortex-pairing as can be seen for vortex no. 3 and no. 4. This phenomenon of loss of downstream speed needs detailed investigation. The exchange with the outer flow is either continuously or

sometimes abruptly. The latter one is called a burst, when the flow is ejected into the outer field. Such a bursting event can be clearly seen in Fig. 5, position C. When you compare positions B and C in Fig. 5 for the vortices no. 1 and no. 4 the rapid change from yellow into deep red evidences the burst phenomenon.

A three-dimensional impression of the vortical structures is obtained using the SPIV technique within a small area of the separation region. The planes are orientated to reconstruct the spanwise structure. Figure 6 displays vector plots of the flow structure in five successive planes at two times of the vortex drift. The time distance between the first and the last image in these vector plots is about 9.9 ms which leads to a scanning speed of 1.84 m/s. This speed suffices for analyzing vortices with a drift speed of $0.6 u_\infty$, since in this study the freestream velocity is $u_\infty = 0.1$ m/s. The results show a definite variation of the vortex structure in the spanwise direction. While in scan no. 1 the rear planes (4, 5) show a large circular vortex, there is no evident circular vortex pattern in the front planes (1, 2). Rather only a vertical motion is visible. In addition, the region of the vertical motion shifts from the front plane to the rear plane, where it is part of the circular vortex, which is, however, located further upstream. Scan no. 2 shows a circular vortex in the typical bursting stage with a pronounced vertical motion in the rear planes (4, 5). In the front plane (1) a region of stronger backflow can be seen, which does not seem to be related to the vortex structure in the rear planes, i.e., it belongs to another vortical structure. Note that this strong variation of the flow structure takes place in the range of $O(2\delta_0)$ in the spanwise direction, i.e., over a distance of approximately 10 mm. As can be seen in the scanning results the bursting vortex can be considered a secondary part of the separation bubble. In fact, another rotating structure can be observed upstream of the bursting vortex, defining the first or inner separation region. It can be conjectured that the drifting vortices form a convex or c-like structure in the streamwise and spanwise directions and therefore, the front scanning planes in scan no. 1 do not cut the vortex core, such that only the roll-up part of the vortex can be seen. Regarding the backflow region in scan no. 2 the spanwise extension of the convex vortices seems to be limited due to other vortices in their vicinity.

Due to the limited depth of focus of the SPIV the total scanning width is limited. Therefore, additional SPIV measurements with horizontal planes parallel to the airfoil surface were taken to visualize the spanwise extension of these vortical structures. In Fig. 7 the lowest scan plane, which is located 0.25 mm above the surface, is shown. This image, being a raw vector plot, gives a good impression of the vortical structures and their spanwise extent. It displays the velocity field, which is not additionally smoothed to not falsify the strong gradients that can also be detected in the planes perpendicular to the surface. Pixel locking did not occur in any of our measurements. To better illustrate the flow the color code from blue to red is used to emphasize the

Fig. 6 Vortical structures in five subsequent scanning planes for two scans with indicated vortex centerline; vectors are drawn with uniform length



upstream (blue) and downstream (red) part of the flow pattern. Furthermore, it can be stated that the upstream orientated vectors form the footprint of the clockwise rotating vortices. As already conjectured from the SPIV measurements with planes perpendicular to the surface, the vortical structures seem to possess a convex or c-like structure when considered in plan view. This structure is indicated with dotted blue lines in Fig. 7. The spanwise extent of the vortex “half-moons” is in the range of 3–7 δ_0 . Further downstream of the vortex structures a region of relatively high downstream velocity can be observed. This can be interpreted as a sweep process where fluid from the main flow is transported towards the wall due

to the vortex circulation. There are in general two subsequent blue regions in the downstream direction, indicating two subsequent vortex structures. As can be clearly seen, there is no regular pattern of the vortex “half-moons” in the spanwise direction. These vortical structures seem to interact with and disturb each other. The small bright blue vectors in the left part of Fig. 7 indicate the footprint of the main recirculation area. These patterns of curved velocity distributions described above were also found by Hain and Kähler (2005) and are interpreted as vortex-“rollers” drifting downstream. Lang et al. (2004) showed phase-locked PIV results in a measurement plane parallel to the surface of a flat plate. The existence of fully counter-rotating vortices observed in their PIV measurements could not be approved.

In Fig. 8 three subsequent planes parallel to the surface are displayed. The upper planes are only partly shown to better illustrate the overall flow pattern. Backflow regions are dominant in the lowest scan plane, while the mean flow direction prevails in the uppermost scan plane. The small regions of backward or low speed flow in the upper planes indicate overlapping or pairing vortices a part of which, e.g., the vortex tips, drifts away from the wall.

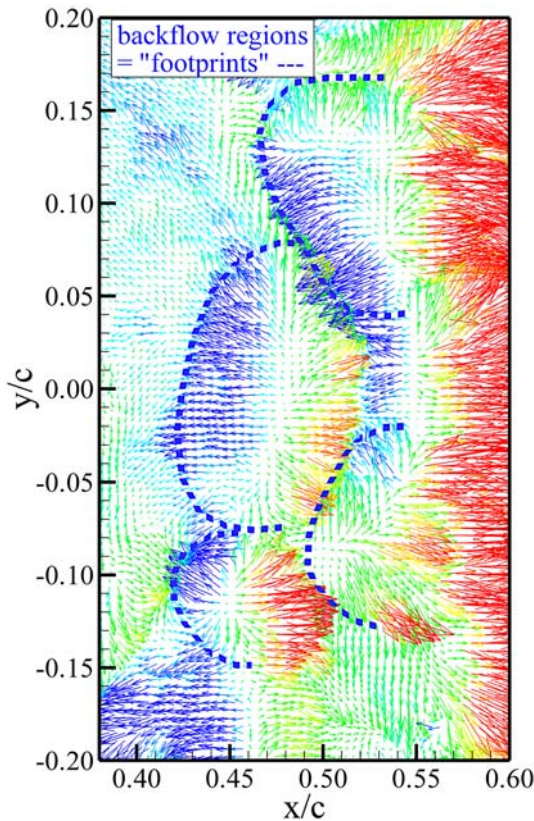


Fig. 7 Footprint of vortical structures in the lowest scan plane close to the airfoil surface

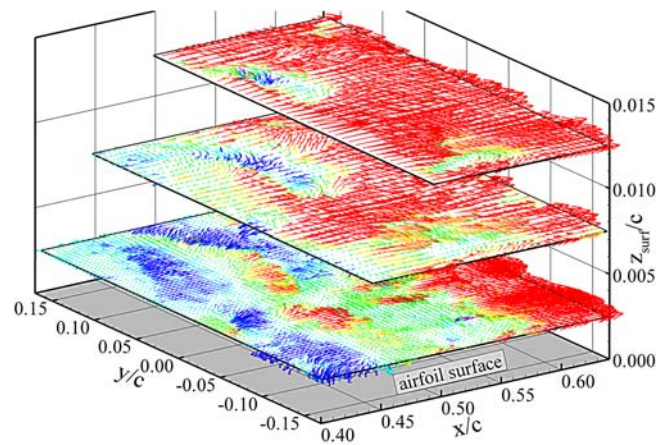
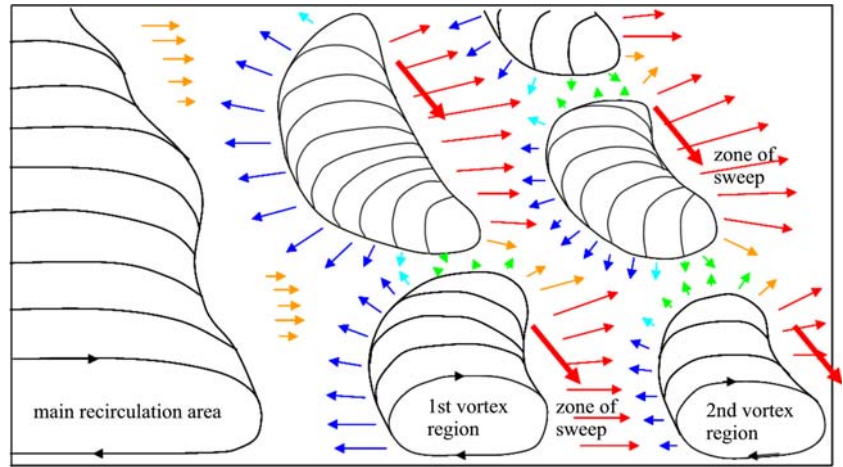


Fig. 8 Scanning planes parallel to the airfoil surface; upper planes are cut for better visibility of vortical structures

Fig. 9 Sketch of vortex footprint and curved vortical structures in the reattachment region



Based on these results a sketch of the vortical structures is drawn that appear in the reattachment zone. As can be seen in Fig. 9 this region can be divided into two major parts: the main recirculation area and the subsequent vortex zone with two vortex regions in the downstream direction. The vortices in these regions show a convex or c-like structure. Downstream of these structures mass from the outer flow impinges upon the wall. The second vortex region is the area where vortex bursting can happen due to a critical size and strength of the vortex. The reattachment line is located on the leeward side of this second vortex region.

4 Discussion

The aforementioned results showed the generating and bursting processes of vortices within the locally separated flow on the suction side of a SD7003 airfoil. The SPIV measurement technique was used to resolve the dynamic vortex behavior and to analyze the spatial extension of the vortex structures within and near the reattachment of the separation bubble. The vortices are formed within the separation bubble as a consequence of the shear layer roll-up due to Kelvin–Helmholtz instabilities and peel away from the main recirculation region, agreeing with the results of Pauley et al. (1990) and Watmuff (1999). These vortices form rather three-dimensional structures so called half-moons than two-dimensional spanwise rolls. The reconstructed spanwise shape evidences convex, i.e., c-like vortices with the lateral arms pointing in the downstream direction. The SPIV measurements confirm that the extension in the spanwise direction can be as small as 10% chord, i.e., $3\delta_0$. In addition, there is no regular pattern of the arrangement of these vortices in the spanwise direction, as has also been shown by Hain and Kähler (2005). Sometimes, the vortices start as large structures and later decompose into smaller units. One distinct feature of these vortices is their tendency to burst abruptly causing a strong vertical fluid motion from the wall into the

mean flow. This behavior is similar to the ejection events in turbulent boundary layer flow. The developed ejection/sweep model gives a rough impression of the vortex structure and the resulting fluid motion near the vortex core and the wall. In this model backflow regions with a convex pattern represent the footprint of the c-like vortex near the airfoil surface. The mechanism to generate these convex structures is assumed to be linked with a fragmentation process of the initial vortex roll due to vorticity differences in the spanwise direction. As observed in our results, the vortex generated within the separation bubble on the one hand increases in size and strength and on the other hand travels downstream and simultaneously reduces its downstream drift speed. The initial drift speed was found to be 60% of the freestream velocity u_∞ , which is in satisfactory agreement compared to 65% determined by Pauley et al. (1990). However, the low speed state is unstable and develops a critical condition, which is assumed to be dominated by the momentum ratio, determined by the accumulation of vortex strength. The vortex rotates as a whole structure around the reattachment point in the downstream direction. This process leads to a strong ejection of low speed fluid into the main flow and acts as a local flow disturbance. This effect is similar to a flow over a hemispherical bump on the surface yielding the deformation of the vorticity line and influencing the upstream roll-up of vorticity. This phenomenon of vortex bursting is not assumed to be the same as the formation of a vortex loop as suggested by Watmuff (1999). Counter-rotating vortex pairs as observed by Lang et al. (2004) were not found in our measurements. This leads to the assumption that the curvature of the airfoil surface has a distinct influence on the development of vortical structures compared to those emerging in a separation bubble due to an adverse pressure gradient on a flat plate. In conclusion, the dynamics of the local separation bubble shows a complex interaction of different phenomena. The sequence of events seems to start with a first instability related to the vortex roll-up in the laminar separation region generating a convex pattern, a growth of

the vortex strength and size until the burst of the vortex with feedback on the upstream flow field occurs.

Acknowledgment This work was funded by the Deutsche Forschungsgemeinschaft within the special focus research program “SPP 1147 Bildgebende Messverfahren für die Strömungsanalyse” (Experimental Visualization Methods for Flow Analysis) under the contract SCHR 309/25-1.

References

- Bastedo WG, Mueller TJ (1986) Spanwise variation of laminar separation bubble on wings at low Reynolds numbers. *J Air* 23(9):687–694
- Brücker Ch (1997) 3-D scanning PIV applied to an air flow in a motored engine using digital high-speed video. *Meas Sci Technol* 8:1480–1492
- Gaster M (1966) The structure and behaviour of laminar separation bubbles. AGARD CP-4, flow separation, Part 2, pp. 813–854
- Hain R, Kähler CJ (2005) Advanced evaluation of time-resolved PIV image sequences. In: 6th international symposium on particle image velocimetry, Pasadena, California, 21–23 September 2005
- Lang M, Rist U, Wagner S (2004) Investigations on disturbance amplification in a laminar separation bubble by means of LDA and PIV. *Exp Fluids* 36(1):43–52
- Maucher U, Rist U, Wagner S (1994) Direct numerical simulations of airfoil separation bubbles. In: Computational fluid dynamics, 2nd ECCOMAS conference, 5–8 September 1994, Wiley, Stuttgart, Germany, pp. 471–477
- McMichael JM, Francis MS (1997) Micro air vehicles—toward a new dimension in flight. URL: http://www.darpa.mil/tto/MAV/mav_aupsi.html, August 1997
- Ol MV, Hanff E, McAuliffe B, Scholz U, Kaehler C (2005) Comparison of laminar separation bubble measurements on a low Reynolds number airfoil in three facilities. In: AIAA Paper 2005–5149, 35th AIAA fluid dynamics conference and exhibit, Toronto, Ontario, 6–9 June 2005
- O’Meara MM, Mueller TJ (1987) Laminar separation bubble characteristics on an airfoil at low Reynolds numbers. *AIAA J* 25(8):1033–1041
- Pauley LL, Moin P, Reynolds WC (1990) The structure of two-dimensional separation. *J Fluid Mech* 220:397–411
- Raffel M, Willert C, Kompenhans J (1998) Particle image velocimetry: a practical guide. Experimental fluid mechanics. Springer, Berlin Heidelberg New York
- Rist U (2002) On instabilities and transition in laminar separation bubbles. In: Proceedings of CEAS aerospace aerodynamics research conference, Cambridge, UK, 10–12 June 2002
- Selig MS, Guglielmo JJ, Broeren AP, Giguère P (1995) Summary of low-speed airfoil data, vol. 1. SoarTech Publications, Virginia Beach, 292 pp
- Wattmuff JH (1999) Evolution of a wave packet into vortex loops in a laminar separation bubble. *J Fluid Mech* 397:119–170